Inhibition of Premixed Methane–Air Flames by Fluoroethanes and Fluoropropanes

G. T. LINTERIS,* D. R. BURGESS, JR., V. BABUSHOK, M. ZACHARIAH, W. TSANG, AND P. WESTMORELAND

National Institute of Standards and Technology, Gaithersburg, MD 20899, USA (G.T.L., D.R.B., V.B., M.Z., W.T.) and University of Massachusetts, Amherst, MA 01003, USA (P.W.)

This paper presents experimental and modeling results for laminar premixed methane–air flames inhibited by the fluoroethanes C_2F_6, C_2HF_5, and $C_2H_2F_4$, and experimental results for the fluoropropanes C_3F_8 and C_3HF_7. The modeling results are in good agreement with the measurements with respect to reproducing flame speeds. For the fluoroethanes, calculated flame structures are used to determine the reaction pathways for inhibitor decomposition and the mechanisms of inhibition, as well as to explain the enhanced soot formation observed for the inhibitors C_2HF_5, $C_2H_2F_4$, and C_3HF_7. The agents reduce the burning velocity of rich and stoichiometric flames primarily by raising the effective equivalence ratio and lowering the adiabatic flame temperature. For lean flames, the inhibition is primarily kinetic, since inhibitor reactions help to maintain the final temperature. The peak radical concentrations are reduced beyond that due to the temperature effect through reactions of fluorinated species with radicals.

INTRODUCTION

The fire suppressant trifluorobromomethane (CF_3Br Halon 1301), discovered in the 1940s [1], is effective [2] and widely used [3]. Unfortunately, it has been found to destroy stratospheric ozone, and its production has been banned [4], creating the need for alternative suppressants. Many of the proposed replacement agents are fluorinated alkanes, and much research is underway both to characterize their performance [5] and to understand their mechanisms of inhibition [6]. The present paper provides experimental data on the reduction in burning velocity of premixed laminar methane–air flames with increasing concentrations of each of the fluoroethanes C_2F_6, C_2HF_5, and $C_2H_2F_4$ (CF_3–CH_2F), and the fluoropropanes C_3F_8 and C_3HF_7 (CF_3–CHF–CF_3), which have been proposed as alternatives to CF_3Br or are important model compounds to study. This work is an extension of previous research on the fluoromethanes CH_2F_2, CHF_3, and CF_4 [7].

Early studies [8–14] on the inhibitory effect of halogenated hydrocarbons on flames were conducted in premixed systems. The premixed laminar burning velocity is a fundamental parameter describing the overall reaction rate, heat release, and heat and mass transport in a flame. Premixed flame burners have flow fields which are relatively easily characterized, making interpretation of the inhibitor's effect on the overall reaction rate straightforward. Although fires are usually diffusion flames, laboratory diffusion flames are believed to have a stabilization region which is premixed [15], and gaining an understanding of the effects of the inhibitors on premixed flames of varying stoichiometries is a useful first step for understanding their chemical effects in diffusion flames. In the present research, burning velocity data allow an examination of the performance of a fluorinated-species kinetic mechanism for hydrocarbon flames developed at the National Institute of Standards and Technology (NIST) [16–18], and permit an examination of the mechanisms of inhibition implied by this reaction set for the inhibitors C_2F_6, C_2HF_5, and $C_2H_2F_4$.

While much recent research [19–24] has been conducted on flame inhibition by the fluoromethanes, comparatively less has been performed on larger fluorinated alkanes. Battin-Leclerc et al. [25] have studied the effect of C_2F_6, C_2HF_5, $C_2H_2F_4$, C_3F_8, and C_3HF_7 on methane and ethane consumption rates in plug-flow and stirred reactors, but found no effect at the low inhibitor concentrations (<1%) of their tests. They also provide some data on the mole fraction of C_2F_6, $C_2H_2F_4$, and C_3F_8 required to

*Corresponding author.

0010-2180/98/$19.00
PII S0010-2180(97)00216-2

Published by Elsevier Science Inc.

produce a 40% reduction in burning velocity, and species profiles from molecular-beam mass spectrometer measurements in low-pressure flames inhibited by C_3HF_7. In related work, Sanogo et al. [26] present the burning velocity reduction in C_2F_6-inhibited methane–air flames, and the structure of low-pressure methane flames inhibited by C_2F_6. Both papers describe numerical modeling of the flames using a kinetic mechanism based on the work of Westbrook [27–29].

The present paper provides a comprehensive set of flame speed data from atmospheric pressure, methane–air flames over a range of equivalence ratios. Experimentally determined burning velocity data are presented for the five inhibitors at nominal values of the fuel–air equivalence ratio ϕ (based on the oxygen demand of the fuel only) of 0.9, 1.0, and 1.1, with inhibitor present in the unburned gases at mole fractions up to 6% (when possible). Numerical calculations of the flame structure and burning velocity are performed for the flames inhibited by the fluoroethanes, and these measurements and calculations provide a basis for interpreting the mechanism of inhibition of the agents. The ability to model these flames will be helpful for their efficient use as fire suppressants, for understanding the unwanted production of hydrogen fluoride (HF) in suppressed fires, and for determining the best conditions for incineration of fluorinated byproducts of chemical production. Although burning velocity data may not be as sensitive a test of a particular reaction mechanism as are flame structure measurements, the burning velocity data of the present research are useful for an early examination of the performance of a fluorinated-species kinetic mechanism developed at NIST [16–18]. The present measurements do have the advantages of more easily covering a wider range of equivalence ratio and inhibitor mole fraction, as well as employing several different inhibitors. Since the burning velocity measurements are performed at atmospheric pressure and at high inhibitor mole fraction, the kinetic mechanisms of inhibition are more directly comparable to those which may occur in the stabilization region of suppressed fires. Methane was selected as the fuel in these first studies in order to avoid the difficulties in modeling the heavily sooting behavior which occurs in inhibited flames of larger alkanes.

EXPERIMENT

Flame speed measurements are performed using a Mache–Hebra nozzle burner [30, 31] which has been described previously [7, 24]. For the present data, the desired equivalence ratio and inhibitor concentration are set and the total gas flow is adjusted to obtain a flame height of 1.3 cm. Maintaining a constant flame height helps to reduce variation in the heat losses from the flame, although some differences remain from the modified final temperatures with inhibitor addition. An optical system provides simultaneously the visible and schlieren images of the flame. A 512 by 512 pixel charged-coupled device (CCD) array captures the image which is then digitized by a frame-grabber board in a laboratory computer. The flame area is determined (assuming axial symmetry) from the digitized schlieren image using image processing software, and the average mass burning velocity for the flame is determined using the total area method [32]. The fuel gas is methane (Matheson UHP); the inhibitors are hexafluoroethane C_2F_6 (Dupont), pentafluoroethane C_2HF_5 and tetrafluoroethane CF_3–CH_2F (Allied Signal), and heptafluoropropane C_3HF_7 and fluoropropane C_3F_8 (Great Lakes Chemical). House compressed air (filtered and dried) is used after it has been additionally cleaned by passing it through an 0.01 μm filter, a carbon filter, and a desiccant bed to remove small aerosols, organic vapors, and water vapor. Gas flows are measured with digitally controlled mass flow controllers (Sierra Model 860)[1] with a claimed repeatability of 0.2% and accuracy of 1%, which have been calibrated with bubble and dry (American Meter Co. DTM-200A) flow meters so that their accuracy is 1%. The burner

[1]Certain trade names and company products are mentioned in the text or identified in an illustration in order to specify adequately the experimental procedure and equipment used. In no case does such identification imply recommendation or endorsement by the National Institute of Standards and Technology, nor does it imply that the products are necessarily the best available for the purpose.

is located in a plexiglas chimney, and there is no co-flowing gas.

The burning velocity in Bunsen-type flames is known to vary at the tip and base of the flame and is influenced by curvature and stretch (as compared to the planar burning velocity); however, these effects are most important over small regions of the flame. The low conductivity of the uncooled quartz nozzle provides low heat loss to the burner, and the low strain and curvature of the flame facilitate comparisons with calculations for a one-dimensional adiabatic flame. The present burner has been shown [7], for near-stoichiometric methane–air flames, to provide final temperatures within 150 K of the calculated adiabatic flame temperature, and flame speeds very close to those obtained by researchers using twin counterflow premixed flames [33]. Although measurement of a true one-dimensional, planar, adiabatic burning velocity (which is what the model describes) is difficult, the relative change in the average burning velocity for the present conical, burner-stabilized flames can be measured with more confidence. Consequently, the burning velocity reduction in the present work is normalized by the uninhibited burning velocity, and the uncertainty in the normalized burning velocities is about 5%.

MODEL

The structures of the premixed methane–air flames inhibited by the two-carbon agents are calculated. The equations of mass, momentum, species, and energy conservation are solved, for the initial gas compositions of the experiments, using the Sandia PREMIX flame code with the Sandia chemical kinetics and transport interpreters [34–36]. The solution assumes isobaric, steady, planar, one-dimensional, laminar flow and neglects radiation and the Dufour effect (concentration gradient–induced heat transfer), but includes thermal diffusion. The Bunsen flames are modeled as freely propagating flames, and the burning velocity is obtained as an eigenvalue of the energy equation. Molecular diffusion is modeled using mixture-averaged diffusion coefficients. The adopted boundary conditions are: inlet mass flux fractions, inlet temperature (298 K), and vanishing gradients downstream. The reaction pathway analyses are carried out using a graphical postprocessor [37].

The calculations employ a chemical kinetic mechanism recently developed at NIST [16–18] for fluorine inhibition of hydrocarbon flames, which is based on earlier work [23, 38, 39]. The 83-species mechanism uses a hydrocarbon submechanism and adds C_1 (200 reactions) and C_2 (400 reactions) fluorochemistry. The hydrocarbon submechanism has been updated to use GRI-Mech 1.2 (31 species, 177 reactions; [40]). The fluorinated-species thermochemistry in refs. [16, 17] is from the literature when available and is otherwise estimated using empirical methods (such as group additivity) and through application of *ab initio* molecular orbital calculations with the (BAC) corrections [41]. Fluorinated species reaction rates from the literature were used when available, for unimolecular reactions in the most general sense, and these were extended to wider temperature and pressure ranges using Rice–Ramsperger–Kassel–Marcus (RRKM) and Quantum Rice–Ramsperger–Kassel (QRRK) methods. Where no rate data were available, rate constants were estimated by analogy with hydrocarbon reactions, and using transition states from *ab initio* molecular orbital calculations with BAC corrections [42]. The comprehensive full mechanism is used for the present calculations (available in a continuously updated form on the World Wide Web [18]). Reduction of the mechanism will be performed later after more experimental validation. It should be emphasized that the mechanism adopted [16, 17] for the present calculations should be considered only as a starting point. Numerous changes to both the rates and the reactions incorporated may be made once a variety of experimental and theoretical data are available for testing the mechanism.

Several reactions, as listed in Table 1, were modified in the present calculations to represent more recent estimations [43]. Although the interrogation of specific reaction rate expressions was directed by the numerical solutions and the comparison of measured and predicted flame speeds, the motivation for the changes was to obtain more accurate rate expressions, not necessarily to increase agreement between

TABLE 1

New Expressions for the Specific Reaction Rate Constant k*

Reaction	A	b	E_a
CO + F + M = CF:O + M	3.09E19	−1.40	−245
CHF_2 + CF_3 + M → CHF_2-CF_3 + M	2.61E26	−4.16	2063
CF:O + CHF_2 = CF_2CO + HF	2.70E13	0.00	10065
CF_3-CHF + H = CHF:CF_2 + HF	6.56E24	−3.57	2125
CF_3-CHF + H = CH_2F + CF_3	4.28E16	−0.74	2400
HCO + CF_3 → CF_2CO + HF	2.70E13	0.00	0.00
CHFCO + F = CF_2CO + H	1.00E13	0.00	0.00

* $k = AT^b e^{-E/RT}$; A = preexponential factor (units: mole-cm-s); T = temperature (K); b = temperature dependence; E/R = activation energy (K) (the third-body efficiencies for the first two reactions are those of GRI-Mech).

burning velocities; some of these changes improve the agreement with the present experimental results, others do not.

RESULTS

Phenomenological Observations

In the absence of inhibitor, the present premixed flames are conical with a bright blue reaction zone. The visible image is straight-sided and parallel to the schlieren image, except at the tip, where the visible image is smoothly curved (the optical arrangement does not provide the schlieren image of the tip). With addition of the inhibitor C_2F_6, the flame remains blue throughout, and the visible and schlieren images are straight-sided for all conditions. Flames could not be stabilized with more than 2% and 4% inhibitor with ϕ equal to 0.9 and 1.1, respectively. With C_2HF_5 addition, the flame is again blue and straight-sided with parallel schlieren and visible images for the lean and stoichiometric flames and were stable up to about 6% inhibitor. Although the rich flames are stable up to about 7% C_2HF_5, the Schlieren image pinches in and becomes more pointed relative to the visible image for C_2HF_5 mole fractions above about 5%, indicating a nonuniform flame speed over the surface of the flame. In contrast to the Schlieren image, the tip of the visible flame becomes rounded and flattened, and is red-orange in color (although the flame does soot excessively). Likewise, the agent $C_2H_2F_4$ forms an orange tip for all equivalence ratios at higher inhibitor mole fractions, but not below 6% $C_2H_2F_4$. Lean and rich flames with this agent blow off at inhibitor mole fractions of about 7% to 10%.

The three-carbon agents C_3HF_7 and C_3F_8 have even more distinct premixed flame appearances. For stoichiometric flames, addition of about 5% C_3HF_7 (or addition of 7% to rich flames) creates a pointed, yellow, sooting conical tip 5 mm high and 1.5 mm wide at the base (about the size of a sharpened tip of a wooden pencil). In contrast, stoichiometric and rich flames with addition of about 4% C_3F_8 have a nonluminous, circular hole, about 2 mm in diameter, at the tip of the premixed flame. For all flames, the pinching in of the schlieren image relative to the visible image and the associated variation of the burning velocity over the surface of the flame is correlated with apparent formation of particulates which emit the orange light. While these phenomena are likely related to the particular chemical decomposition pathways of the hydrofluorocarbons, comparisons of the measured and calculated flame speeds will be restricted to lower inhibitor loadings where the uncertainties associated with nonuniform burning velocities and soot formation can be avoided. Calculations performed for the two-carbon inhibitors at mole fractions below 6% are used to interpret the strong sooting behavior of C_2HF_5, $C_2H_2F_4$, and C_3HF_7.

Burning Velocities

The burning velocities of the uninhibited flames are in good agreement with both the results of other researchers and the predictions of the numerical calculations using GRI-mech. As previously discussed [7], for $0.8 \leq \phi \leq 1.2$ the

measured flame speed from the present apparatus is only 3% to 7% higher than those recently reported by Vagelopoulos et al. [33], which are in excellent agreement with the calculated burning velocities using GRI-Mech.

The measured and calculated burning velocities in the presence of the two-carbon inhibitors C_2F_6, C_2HF_5, and $C_2H_2F_4$ and for nitrogen are presented in Figs. 1–3. The burning velocities shown in the figures are normalized by the uninhibited value for each inhibitor as listed in Table 2 (the different values of the burning velocity for a given value of ϕ in this table show the experimental scatter). In Figs. 1–3, the points represent the experimental data for values ϕ of 0.9, 1.0, and 1.1, while the solid lines present the corresponding predictions from the numerical calculations with full chemistry. The excellent agreement between the calculated and measured burning velocity reduction for nitrogen as an inhibitor (straight lines and data in Fig. 1) reflects the good performance of GRI-Mech.

For the fluorinated inhibitors, Figs. 1–3 show that a two-thirds reduction in the burning velocity is achieved with about 4% to 5.3% of the two-carbon inhibitors for the stoichiometric flames. For comparison, these stoichiometric flames blow off at 4% to 9% inhibitor (as discussed in the previous section). The rich flames are inhibited most, and for a given inhibitor, the difference between the inhibitor effectiveness for the rich and lean flames is greater for agents with increased hydrogen content. (This is discussed further below.) The measured burning velocities of the methane–air flames inhibited by the three-carbon inhibitors C_3F_8 and C_3HF_7 are given in Figs. 4 and 5. The perfluorinated agent C_3F_8 behaves much like C_2F_6, producing the most burning velocity reduction, about 80% at 4% inhibitor, and the least variation in the magnitude of the inhibition with ϕ. The agent C_3HF_7 has significant variation in its inhibition effectiveness with ϕ as do the two-carbon hydrofluorocarbons. It is anomalous, however, in that the stoichiometric flame provides the most inhibition rather than the rich flames as for all other agents tested.

Apparently, rich premixed flames are inhibited more strongly than lean flames as indicated here by the agents C_2F_6, C_2HF_5, $C_2H_2F_4$, and C_3F_8. This behavior is also indicated by the data of Rosser et al. [14], in which over a narrow range of ϕ, CF_3Br inhibits methane–air flames more strongly for rich ($\phi = 1.1$) flames than for lean ($\phi = 0.9$). Since lean flames are more deficient in H-atoms and since halogens generally are believed to inhibit flames by reducing H-atom concentrations, one might expect lean flames to be inhibited more. This is indeed the case for inhibition by Br_2 [14] in which lean flames are inhibited slightly more strongly (4%) than rich flames, and also for methane–air flame inhibited by $Fe(CO)_5$ [44], in which lean flames are also inhibited more strongly (about two times) than rich flames. In lean flames, the weaker inhibition by CF_3Br and the fluoromethanes listed above is likely due to the fuel effect of adding these agents (which are fuel-like) to lean flames (and the resulting increase in the final temperature as discussed below).

As Figs. 1–3 for the two-carbon inhibitors illustrate, with inhibitor mole fractions of less than 3%, the full-chemistry model predicts the burning velocities exceptionally well, within a few percent for all three inhibitors at all values of ϕ. At the highest inhibitor loadings of the experiments, however, the model tends to over-predict the burning velocity reduction. For C_2F_6 and C_2HF_5, this over-prediction of the inhibition occurs only for the rich flames, where it is up to 14%, whereas for $C_2H_2F_4$ it is about 8% for all values of ϕ. These discrepancies at higher inhibitor loading indicate that further development of the mechanism is warranted, particularly the inclusion of three-carbon compounds. Nonetheless, the agreement in Figs. 1–3 is excellent considering the early stage of model validation, the complexity of the reaction set, and the estimations necessary for its development.

Figure 6 presents the experimentally determined burning velocity reductions for all of the inhibitors at stoichiometric conditions, together with the results for CF_3Br in stoichiometric flames from Rosser et al. [14]. In this figure, curve fits to the experimental data are shown. Also plotted are the calculated burning velocity reductions with ethane added to rich and lean methane–air flames. As the figure indicates, CF_3Br is superior to all of the agents, by a factor of about five for C_2HF_5 and $C_2H_2F_4$ which are

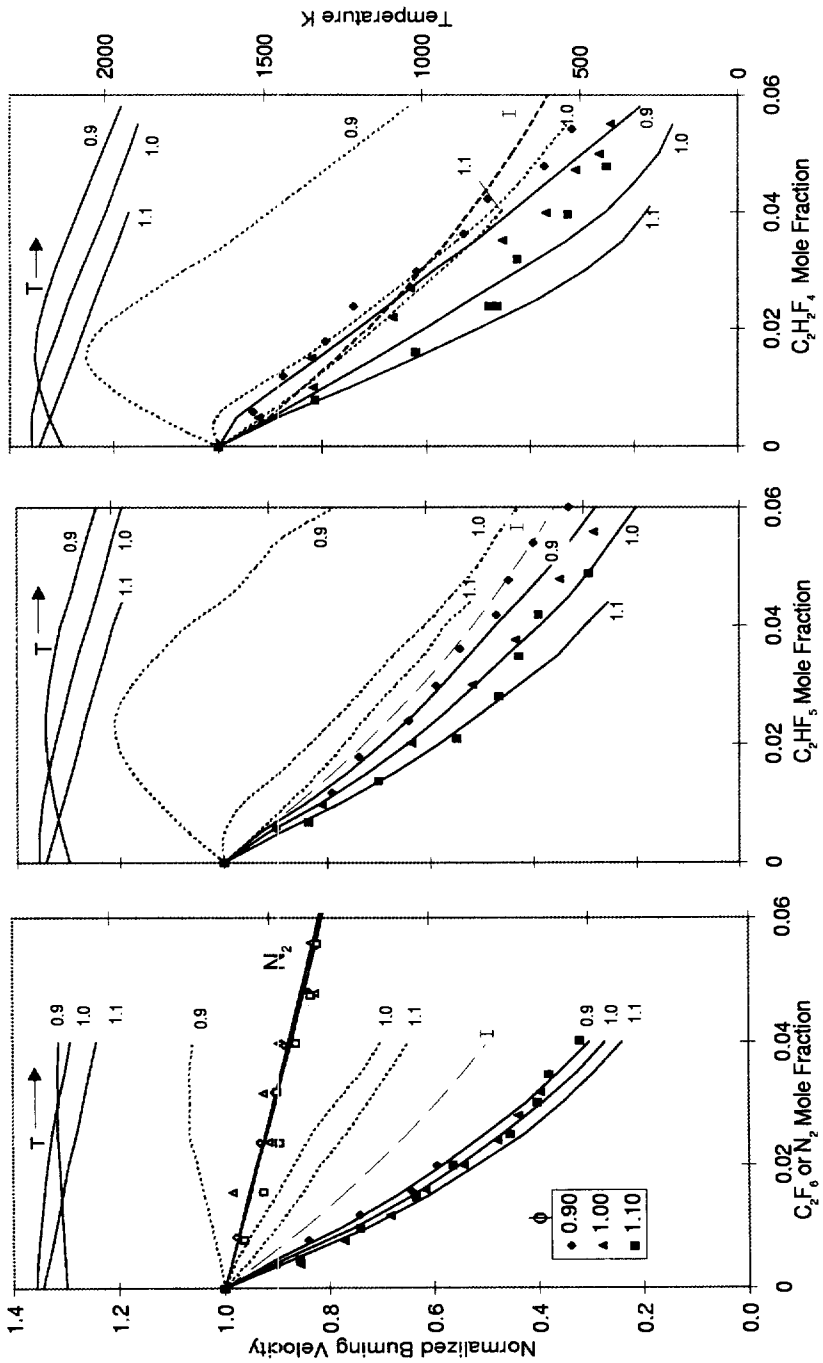

Figure 1

Figure 2

Figure 3

Fig. 1–3. Burning velocity of premixed methane–air flame normalized by the uninhibited burning velocity at the same stoichiometry as a function of the inhibitor mole fraction of the total reactant stream. Data are presented for the inhibitors N_2 and C_2F_6, C_2HF_5, and $C_2H_2F_4$, at fuel–air equivalence ratios of 0.9, 1.0, and 1.1. The open symbols present the experimental data, the solid lines the results of the numerical calculation allowing inhibitor reaction, and the dotted lines, the results of the numerical calculation for uninhibited methane–air flames but at the equivalent final temperature of the inhibited flames. The dashed lines next to the letter I present the calculated burning velocity for $\phi = 1.0$ when the inhibitor is present but inert.

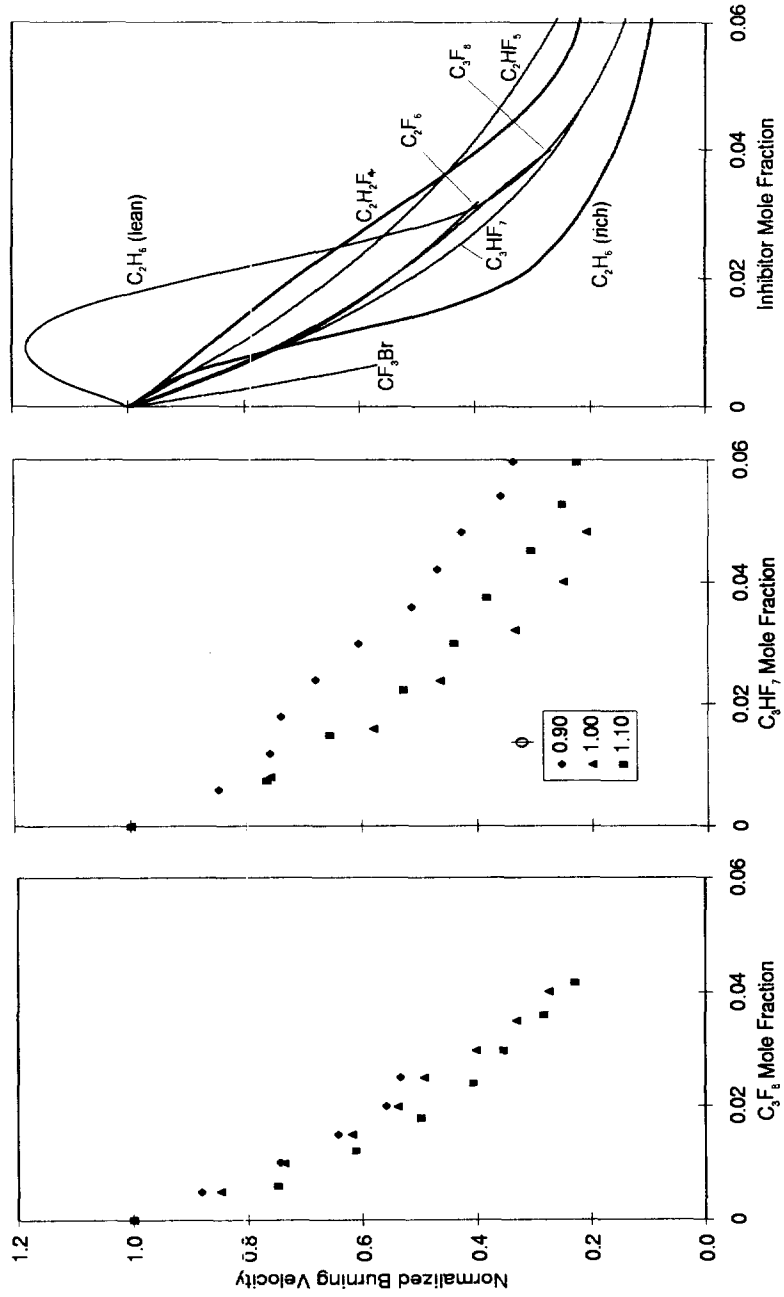

Figure 4 Figure 5 Figure 6

Fig. 4–6. Burning velocity of premixed methane–air flame normalized by the uninhibited burning velocity at the same stoichiometry as a function of the inhibitor mole fraction of the total reactant stream. Experimental data are presented for the inhibitors C_3F_8 and C_3HF_7 at fuel–air equivalence ratios of 0.9, 1.0, and 1.1. Fig. 6 shows curve fits to the experimental data for the five inhibitors and CF_3Br for $\phi = 1.0$, and for ethane with $\phi = 0.9$ and $\phi = 1.1$.

TABLE 2

Values of the Measured and Calculated Burning Velocities of Uninhibited Premixed Flames as a Function of Equivalence Ratio Used for the Normalizations in Figs. 1–6.

	Burning Velocity, cm/s		
	Φ		
Case	0.9	1.0	1.1
C_2F_6	36.8	41.9	39.1
C_2HF_5	37.8	42.3	38.3
$C_2H_2F_4$	37.3	41.2	39.2
C_3F_8	37.7	40.0	40.9
C_3HF_7	37.3	42.0	40.4
Model	35.5	40.0	40.3

nearly equivalent, and by about four for C_2F_6, C_3HF_7, and C_3F_8 which are also nearly equivalent. Interestingly, under some conditions, the slope of the reduction in burning velocity with ethane addition is about equal to that for CF_3Br addition. The self-inhibiting effect of fuel addition, in which the hydrocarbon species competes with O_2 for reaction with H-atom to reduce the branching ratio, has been described in many places in the literature, for example, ref. [45]. In addition, a chemical mechanism for radical recombination, where the pertinent reactions are:

$$H + CH_3 + M \rightleftharpoons CH_4 + M$$

$$H + CH_4 \rightleftharpoons CH_3 + H_2$$

$$(\text{net: } H + H \rightleftharpoons H_2)$$

has been proposed by Benson [46]. Finally, most of the important reactions of the CH_3 radical are chain-terminating; e.g.,

$$CH_3 + CH_3 \rightleftharpoons C_2H_6$$

$$CH_3 + O \rightleftharpoons CH_2O + H$$

$$CH_3 + CH_3 \rightleftharpoons C_2H_4 + H_2$$

$$CH_3 + H + M \rightleftharpoons CH_4 + M,$$

so that higher methyl radical concentrations from richer flames lead to greater radical chain termination steps and reduced burning velocities.

DISCUSSION

Temperature

These inhibitors have sometimes been described as acting physically to suppress fires through the reduction in final temperature. Methods have been devised to describe these physical effects through consideration of the specific heat of the intact inhibitor molecule [25, 47, 48], and to estimate the fraction of the total inhibition resulting from physical effects [48, 49]. Considering the complete decomposition of these inhibitors in premixed flames [50], however, the heat release (positive or negative) from reaction of the inhibitor must be considered, as well as their effect on the final products. These two effects combine to influence the heat release per unit mass and hence the adiabatic flame temperature and burning velocity. Consequently, it is of interest to examine the effect of agent addition on the flame temperature, with the goal of assessing how much of the actual burning velocity reduction may be attributable to temperature reduction.

The calculated final temperature (adiabatic flame temperature) of the flames as a function of the inhibitor mole fraction is given for each value of ϕ by the upper set of curves in Figs. 1–3. As the figures illustrate, all lean flames experience an increase in the adiabatic flame temperature with addition of the inhibitor, up to 200 K for C_2HF_5 and $C_2H_2F_4$, but only about 100 K for C_2F_6. The stoichiometric and rich flames experience a decrease in adiabatic flame temperature of up to 300 K with addition of inhibitor. Note that the increase in flame temperature for lean flames (and decrease for rich flames) is greater as the hydrogen to fluorine ratio in the inhibitor increases; i.e., as the agent becomes more of a fuel (since fluorine is an oxidizing species).

Comparisons of the calculated burning velocity reduction with inhibitor addition for both full chemistry and with the inhibitor constrained to be inert have been performed previously for the fluoromethanes [7]. Although these comparisons allow an assessment of the additional inhibition obtained with the actual inhibitor beyond that which would have occurred *if* the agent were inert, they neglect the heat release from

the agent reaction. The approach for comparison in the present paper is based on the calculated final temperature of the inhibited flame, and allows inclusion of the combined influence of the heat capacity and heat release of the agent. By calculating the burning velocity of a pure methane/oxygen/nitrogen flame at the equivalent final temperature of the inhibited flame, and comparing this value with the burning velocity of the inhibited flames calculated with full chemistry, the effect of the inhibitor beyond that due to temperature reduction (or gain) can be determined.

In Figs. 1–3, the dotted curves show the calculated burning velocity of a pure methane–air flame with values of ϕ of 0.9, 1.0, and 1.1, but at the final temperature of the inhibited flames (higher final temperatures for these uninhibited flames are obtained by reducing the nitrogen content of the oxidizer in the calculations, while lower temperatures are obtained by adding C_2F_6 as an inert species). The effect of inhibitor reaction on the temperature is described below, and the influence on radical concentrations is described in a later section. For comparison, the dashed line (marked I) shows the burning velocity of a stoichiometric flame with addition of agent as an inert species (such inert addition to lean and rich flames gives normalized burning velocities which are very close to this curve).

For lean flames with the three fluoroethanes, the adiabatic flame temperature increases for many of the conditions shown in Figs. 1–3, as does the burning velocity at the equivalent final temperature. Nonetheless, the burning velocity is always decreased with addition of the fluoroethanes to lean flames. Consequently, for many of the conditions of the present lean flames, it appears that there is no reduction in the burning velocity from a lowered temperature, but rather, from kinetic mechanisms only.

The rich and stoichiometric flames of the fluoroethanes behave somewhat differently: the lower temperatures which occur with addition of the agent reduce the burning velocity 30% to 50% with 4% inhibitor, whereas, with the agent present but inert (dashed lines, I label), the burning velocity is reduced more, about 50% for all cases. That is, reaction of the inhibitor, even for rich and stoichiometric flames of C_2F_6 and C_2HF_5 (but not $C_2H_2F_4$), provides additional heat release, and based on the final temperature, the burning velocity would be higher than if the agent were inert. Nonetheless, for all three agents, the calculated burning velocity with full chemistry is always lower than that based only on the final temperature (or calculated with an inert agent), illustrating the chemical inhibition of the flame chemistry. Hence, when assessing the physical and chemical contributions of a particular inhibitor to burning velocity reductions, it is important to consider not only the lowered temperature due to the added mass of the inhibitor, but also its heat release upon reaction. When this is done, the implications for the relative role of thermal versus chemical effects vary, especially at lower equivalence ratios.

Radical Concentrations

Brominated inhibitors such as CF_3Br and HBr are believed to reduce the burning rates of flames by reducing the H-atom concentration in the reaction region [27–29, 51, 52]. In this mechanism, H atoms catalytically recombined to form H_2 through a sequence involving the bromine atom. Fluorinated compounds, although they are believed to suppress the H-atom concentration and reduce chain branching through termination steps involving HF formation [20, 29, 53, 54], are not believed to enter into the highly effective catalytic cycles characteristic of brominated compounds. In order to understand the effect of fluorinated compounds on the radical pool in flames, it is of interest to examine the decrease in radical concentrations with addition of fluorinated inhibitors. Various locations in the flame have been used for assessment of the effect of inhibitors on chain carrier concentrations, including the radical mole fractions at the point of half fuel consumption, inflection point in the temperature curve, maximum heat release, 95% fuel consumption, as well as the peak radical mole fraction. Unfortunately, there exists no generally accepted location for comparison of the strength of chemical inhibition by different agents. For the radicals O, H, and OH, we present the calculated mole fraction at the point of 95% fuel consumption. As described below, we also present the peak

value and equilibrium value in the final product gases.

The radical concentration in the main reaction region of the flame is of interest since it is here that lower radical mole fractions lead to less chain branching, and lower the consumption rate of the fuel. In the present flames, the point of 95% fuel consumption is close to the location of maximum reaction rate and the inflection point in the temperature curve, so this location is examined. Peak and equilibrium values are generally of interest since the difference between the two provides the driving force for radical recombination; that is, lowered radical super-equilibrium renders catalytic agents less effective. An important difference between these fluorinated agents and agents believed to act catalytically such as $Fe(CO)_5$ and CF_3Br is that since large amounts of the fluorinated agents are added, they change dramatically the equilibrium mole fractions of the radicals, particularly O and OH, in the final products. In the present paper, the peak and equilibrium mole fractions of O, H, and OH, as well as the mole fractions of these radicals at the point of 95% fuel consumption are presented for flames with added fluoroethanes as well as with added CF_3Br. The numerical results for the latter are obtained from the calculations in ref. [49].

The peak and equilibrium radical concentrations in stoichiometric CH_4–air flames for CF_3Br and for the three fluoroethanes are illustrated in Figs. 7–10. The top part of each figure presents the *equilibrium* mole fraction of H, O, and OH at the calculated adiabatic flame temperature as a function of the inhibitor mole fraction in the reactant stream, while the lower part of each figure presents the corresponding curves for the *peak* value of the radical mole fractions. The radical mole fractions at the point of 95% fuel consumption are given by Figs. 11–14. In these curves, the solid lines show the calculated radical mole fractions, and the dotted lines show the radical mole fractions of a pure methane/oxygen/nitrogen flame at the equivalent final temperature of the inhibited flame (calculated as described above). Since addition of the inhibitor to stoichiometric flames acts to both change the chemical environment of the flame and change (usually lower) the flame temperature, these plots help to illustrate the magnitude of each effect (thermal and chemical) on the peak and equilibrium radical mole fractions and the values at the point of 95% fuel consumption.

Figure 7 illustrates the results for flames with CF_3Br. (Note that a CF_3Br mole fraction of 0.025 corresponds to an 80% reduction in the burning velocity.) In Fig. 7, the equilibrium mole fractions of O, H, and OH are shown to be lowered by a factor of two due to the lower temperature of the inhibited flames (dotted lines), while the chemical effect of the CF_3Br itself has very little additional effect on the equilibrium values. For the fluoroethanes (Figs. 8–10), the equilibrium mole fractions of O, H, and OH are all lowered equivalently by the lower temperatures of the inhibited flames (dotted lines), although the effect is slightly stronger for the inhibitors with higher hydrogen content. In contrast, additional lowering (solid lines) of the equilibrium radical mole fractions beyond that due to the lowered temperature (dotted lines) is very important for the fluoroethanes: equilibrium O and OH concentrations are one to two orders of magnitude lower than that due to the temperature effect, while H concentrations are actually higher than one would expect based on the final temperature, and only slightly lowered from the uninhibited case; i.e., the inhibited flames act as richer flames, with lower equilibrium concentrations of oxygenated radicals (especially true as the hydrogen content of the inhibitor increases).

The effect of inhibitor addition on the *peak* radical mole fractions (bottom of Figs. 7–10) shows that the relative reduction in the peak mole fractions is greater than for equilibrium values for CF_3Br while for the fluoroethanes, the peak values are reduced less than the equilibrium values (note the scale change in the figures). For CF_3Br the peak H-atom mole fraction is reduced the most, while for the fluoroethanes, as the hydrogen content of the agent increases, the H-atom mole fraction is decreased the least. The reduction in peak radical mole fractions due to the lowered temperatures is much smaller than the reduction in the equilibrium values.

For the calculated radical mole fractions at the point of 95% fuel consumption (Figs. 11 to 14), several observations can be made. For

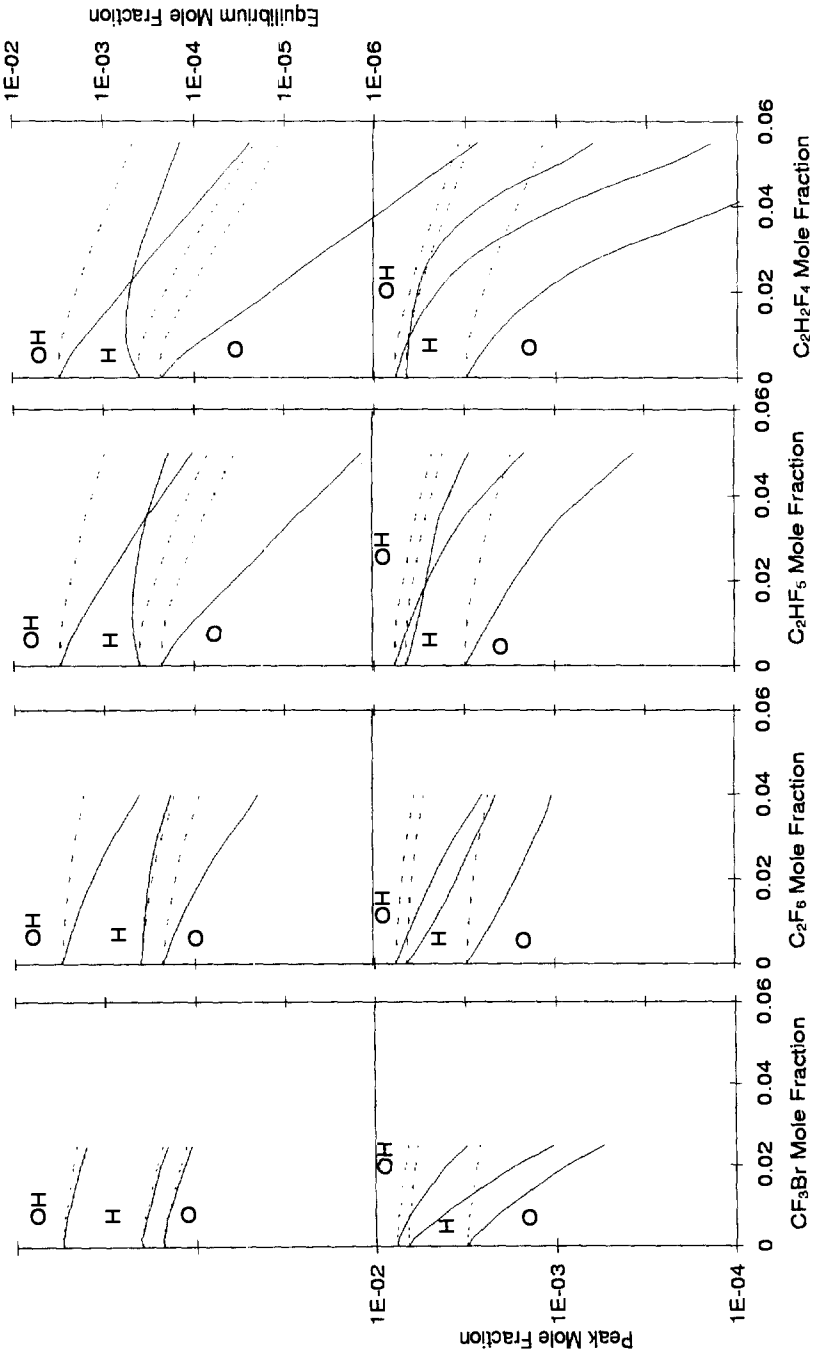

Fig. 7–10. Numerically calculated equilibrium (upper half of figures) and peak (lower half) O, H, and OH mole fractions (solid lines) as a function of inhibitor mole fraction in the total reactant stream for CF_3Br, C_2F_6, C_2HF_5, and $C_2H_2F_4$, added to a stoichiometric methane–air flame. Also shown (dotted lines) are the equilibrium and peak mole fractions of O, H, and OH in a methane–air flame at the same final temperature of the inhibited flame (obtained through addition of small quantities of an inert species or a small increase in the oxygen mole fraction in the calculations).

Figure 7 Figure 8 Figure 9 Figure 10

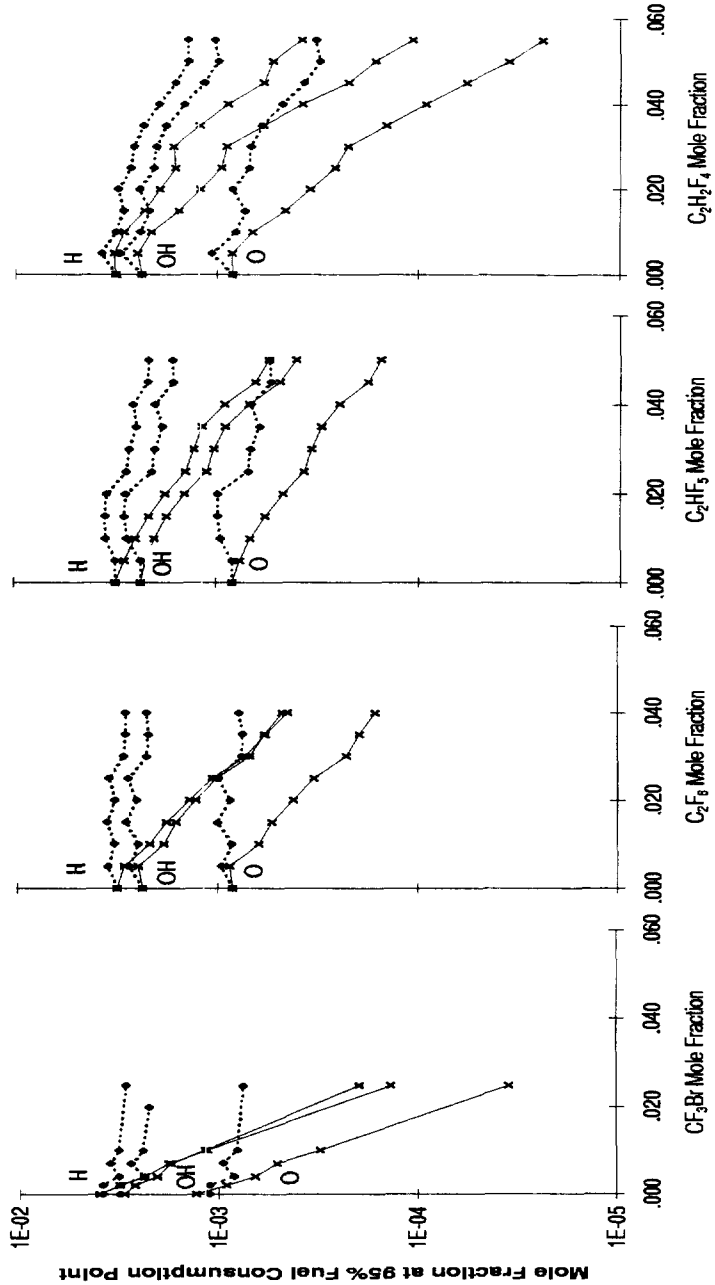

Figure 11 Figure 12 Figure 13 Figure 14

Fig. 11–14. Numerically calculated O, H, and OH mole fractions at the point of 95% fuel consumption (solid lines) as a function of inhibitor mole fraction in the total reactant stream for CF_3Br, C_2F_6, C_2HF_5, and $C_2H_2F_4$, added to a stoichiometric methane–air flame. Also shown (dotted lines) are the values in a methane–air flame at the same final temperature of the inhibited flame (obtained as described above).

CF_3Br and all the fluorinated agents, the lower final temperatures (dotted lines) reduce O, H, and OH equivalently and mildly. For CF_3Br (Fig. 11), the chemical effect of the agent (solid lines) strongly reduces the chain carrying radical mole fractions in the reaction zone; likewise, for the fluorinated agents, there is additional reduction (solid lines) from chemical effects beyond that due to the lowered final temperatures. As the hydrogen content of the inhibitor increases, the reduction in the oxygenated radicals O and OH is greater than for hydrogen atom; for C_2F_6 the reduction for the three radicals is equivalent. Hence, addition of fluorinated inhibitors reduces the chain carrying radical mole fractions in the reaction zone primarily because of chemical rather than thermal effects.

Reaction Pathways

From the numerical calculations, the rate of each reaction can be integrated over the entire flame to produce the flux of each reaction. For each species, the most important reactions leading to its consumption can be determined, to provide the reaction pathway for consumption of the inhibitor molecule.

These pathways, determined for stoichiometric flames with 2% C_2F_6, C_2HF_5, and $C_2H_2F_4$ are shown in Figs. 15, 16, and 17, respectively. In these figures, the arrows connect species of interest. Next to the arrows are the reaction partners and, in parentheses, the percent of the parent species that reacts through that route (for 2% inhibitor). Where there is a significant change in the relative contributions with inhibitor loading, two values are given corresponding to 2% and 4% inhibitor. Although these figures are somewhat complicated, they attempt to summarize the chemistry occurring in a reaction mechanism containing nearly 100 species and 1000 reactions; with some patience, the figures can be useful for understanding the dominant routes of inhibitor consumption and for determining the next group of reactions for more detailed consideration in model development.

For C_2F_6 (Fig. 15), the inhibitor undergoes thermal decomposition to form two CF_3 radicals, so that the pathway is very similar to that described previously [7] for CHF_3, which also predominantly forms CF_3 in its consumption. In both cases, about 20% of the fluorine is rapidly incorporated into two-carbon fluorinated species (although the C_2F_6 forms some directly whereas with CHF_3, it is all by CF_3 reaction with CH_3). As in inhibition by CHF_3, the CF_3 is consumed mostly through radical attack by H to form CF_2 and to a lesser extent by O and OH to form CF_2:O (which decomposes slowly in the flame by reaction with H, and persists for almost a centimeter into the postcombustion gases). The CF_2 then reacts with H to form CF, which is consumed by reaction with O_2 or OH to form CF:O or CO. This last species reacts with H and OH or through thermal decomposition, with the latter route dominating.

For the agent C_2HF_5 (Fig. 16), thermal decomposition is again the dominant route of initial destruction, in this case through HF elimination to form CF_2:CF_2, while hydrogen abstraction to form CF_3–CF_2 accounts for about a quarter of the C_2HF_5 consumption at low inhibitor loading, but less at higher. Through either route, the two-carbon intermediates CF_2:CF_2 and CF_3–CF_2 form, and react primarily with radicals to form CF_3, CF_2, and CHF_2. These former two species are consumed as in C_2F_6 oxidation as described above, while CHF_2 is consumed as in the reaction pathway described previously for CH_2F_2 [7]. A quarter to half of the CHF_2 reacts with CH_3 to form two-carbon fluorinated species or CF_2, while 20% to 45% reacts with H to form CHF, which reacts mostly with H to form CH. It is noteworthy that the model shows consumption of CH (formed from both CH_4 and inhibitor oxidation) to occur mostly through reaction with HF, a species which is often thought to be a stable final product in these inhibited flames.

It is interesting to observe that both of these C_2HF_5 premixed flames and flames of CH_2F_2 [55] which decompose through CHF_2 are the cases that also appear to form soot (as indicated by the observed yellow or orange luminous region in downstream region of the flame), while neither the C_2F_6 nor the CHF_3 flames, which proceed through CF_3 form soot. It has been noted [56] that several researchers [57–59] have proposed a soot formation route in methane–air flames involving C_3H_3, in which this species is formed by acetylene reaction with CH. The present results support such a mecha-

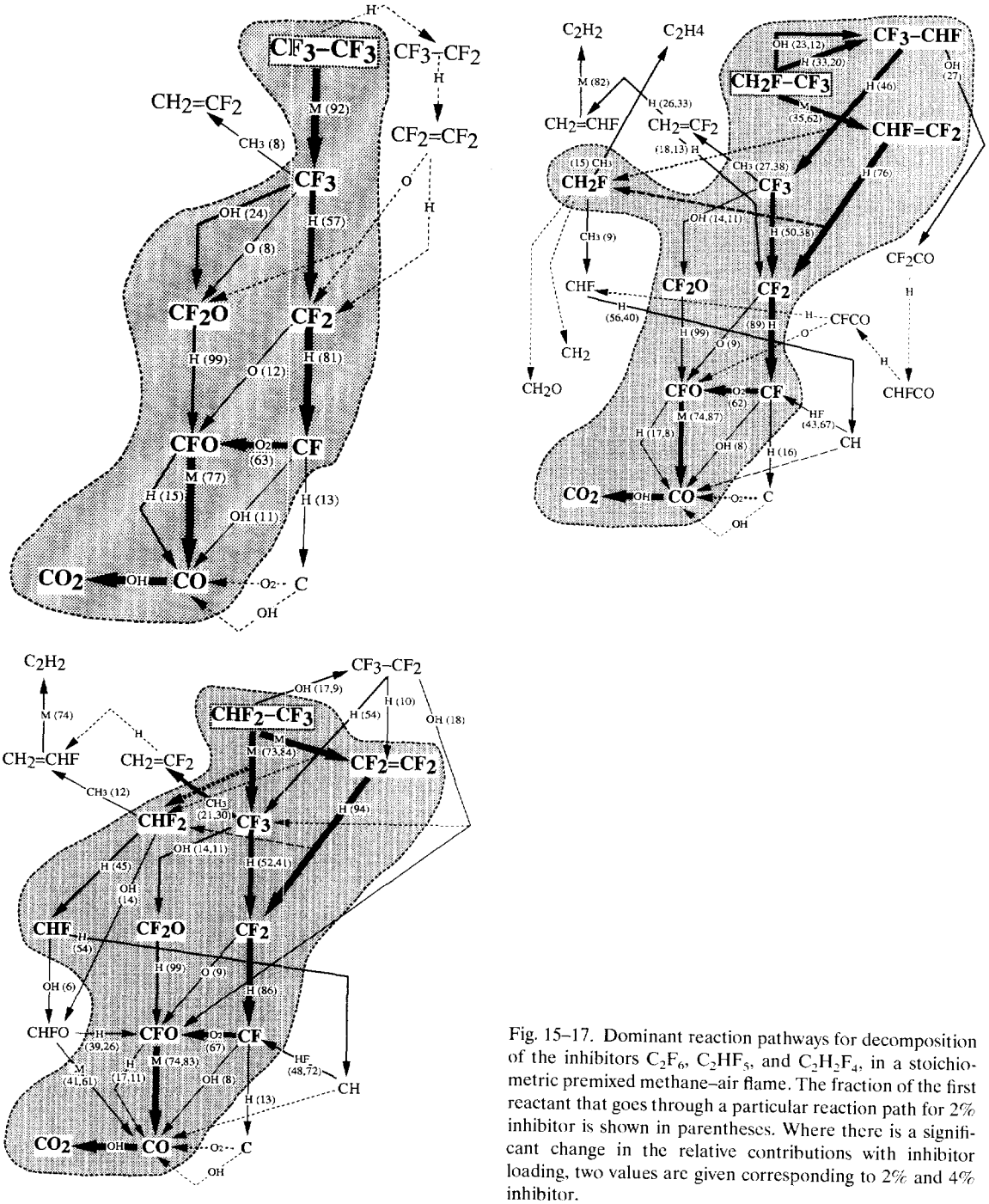

Fig. 15–17. Dominant reaction pathways for decomposition of the inhibitors C_2F_6, C_2HF_5, and $C_2H_2F_4$, in a stoichiometric premixed methane–air flame. The fraction of the first reactant that goes through a particular reaction path for 2% inhibitor is shown in parentheses. Where there is a significant change in the relative contributions with inhibitor loading, two values are given corresponding to 2% and 4% inhibitor.

nism, since decomposition of CHF_2 leads to CH formation. Also, an important source of acetylene in both the present C_2HF_5-inhibited flames and CH_2F_2-inhibited flames is the HF elimination from CH_2:CHF. This latter species forms readily from CHF_2 reaction with CH_3, as well as from decomposition of other two-carbon fluorinated species.

Referring to Fig. 17, initial breakdown of the agent $C_2H_2F_4$ is also dominated by either HF

elimination or radical attack to form $CHF{:}CF_2$ or CF_3–CHF, respectively, with the elimination route favored at higher inhibitor loading. Most of the $CHF{:}CF_2$ reacts with H to form CH_2F and CF_2, while half of the CF_3–CHF also reacts with H to form CH_2F as well as CF_3. The species CH_2F reacts with various radicals to form HF and hydrocarbons, and with CH_3 to form ethylene (which leads to acetylene formation) and CHF (which leads to CH). Consumption of the CF_3 occurs as in the inhibitors described above; however, the fraction pyrolyzing with CH_3 to form $CH_2{:}CF_2$ is higher, and much of this species forms $CH_2{:}CHF$ and then acetylene. Hence, with this agent, the routes to C_2H_2 formation are even stronger than with C_2HF_5 described above. These results are consistent with the even stronger observed sooting tendency for this agent.

In previous research, the agent $CF_2{:}O$ has been found to decompose slowly and persist into the post combustion gases [23]. For the present flames, however, it is an important intermediate only for C_2F_6. As the hydrogen content of the inhibitor increases, the pathway proceeds less through $CF_2{:}O$ so that the peak $CF_2{:}O$ mole fraction for flames inhibited by $C_2H_2F_4$ is an order of magnitude less than for flames with C_2F_6 and the $CF_2{:}O$ is also consumed faster.

CONCLUSIONS

The reduction in burning velocity has been determined experimentally and numerically for the fluorinated inhibitors C_2F_6, C_2HF_5, and $C_2H_2F_4$, and experimentally for C_3F_8 and C_3HF_7, in near-stoichiometric ($0.9 \leq \phi \leq 1.1$) premixed methane–air flames at inhibitor concentrations up to 6% (which is a significant fraction of the blow-off concentration). These data and calculations represent the first comprehensive set of such data for these agents, fuel, and conditions. The NIST fluorine-inhibition mechanism predicts the burning velocity reduction quite well, within a few percent, for inhibitor mole fractions up to 3% and all values of ϕ. For higher inhibitor loadings and rich flames, the mechanism tends to over-predict the inhibition by 8% to 14% for the three fluoroethanes. Further research is necessary to test the mechanism using data from other experimental configurations, such as detailed flame structure measurements.

Although the burning velocity is always reduced with inhibitor addition to the present flames, the adiabatic flame temperature is sometimes increased, especially for lean flames and inhibitors with high hydrogen to fluorine ratios. When assessing the relative contributions of physical and chemical properties of the agents to flame inhibition, both the added mass and the additional heat release must be considered (i.e., their net effect on the final temperature). Numerical calculations at an equivalent final temperature of the experiments show that for the lean flames, inhibition occurs only through chemical kinetic effects for many conditions.

Unlike agents such as CF_3Br which are believed to have a strong catalytic radical recombination action, these fluorinated agents cause a strong reduction in the equilibrium mole fraction of chain carrying radicals O, H, and OH, and a more mild, but clear, reduction in the peak mole fraction and the mole fraction near the reaction zone. For these latter two locations, the reduction in the mole fractions are seen to occur mostly from chemical kinetic rather than thermal effects. As the hydrogen content of the inhibitor increases, the oxygenated radical mole fractions are more reduced by inhibitor addition than is hydrogen atom.

In the present premixed flames, the agents CHF_3, C_2F_6, and C_3F_8 are found to be nonsooting even at high inhibitor mole fractions, whereas CH_2F_2, C_2HF_5, $C_2H_2F_4$, and C_3HF_7 are soot-forming. Examination of the reaction pathways for the one- and two-carbon inhibitors shows significant differences in their decomposition routes, which may account for their sooting behavior. The former group of agents (CHF_3 and C_2F_6) decompose primarily via $CF_3 \rightarrow CF_2 \rightarrow CF \rightarrow CF{:}O \rightarrow CO$, whereas the second group (CH_2F_2, C_2HF_5, and $C_2H_2F_4$) predominantly form CHF_2 and CH_2F which are more prone to form CHF, CH, CF, and CF:O. This latter group may more readily form soot through a three-carbon production route involving CH and acetylene.

The reactions for inhibitor consumption

change significantly at low and high inhibitor loading. At low inhibitor mole fraction, the inhibitors and their fragments are consumed primarily by radical attack, whereas, at high mole fraction, pyrolysis reactions with CH_3 to form larger fluorinated species are very important, as are thermal decomposition reactions. These differences may account for the lower change in burning velocity with addition of inhibitor as the inhibitor mole fraction increases.

This research was supported by the U.S. Naval Air Systems Command, U.S. Army Aviation and Troop Command; Federal Aviation Administration Technical Center, and the U.S. Air Force. The authors are grateful to Kermit Smyth for helpful conversations about soot formation, to Drs. J. Vandooren and P. Van Tiggelen for helpful suggestions concerning the experimental techniques, and to Dr. J. Hodges for help with the image processing. Lenny Truett and Arnold Liu made significant contributions to the experimental research.

REFERENCES

1. Purdue University (1950, July). *Final Report on Fire Extinguishing Agents for the Period 1 Sept. 1947 to 30 June 1950*. Purdue University Foundation and Department of Chemistry, West Lafayette.
2. Gann, R. G., Ed., *Halogenated Fire Suppressants*. ACS Symposium Series No. 16, American Chemical Society, Washington, DC, 1975.
3. Anderson, S. O., *Fire J.* 81(56):118 (1987).
4. *Scientific Assessment of Stratospheric Ozone: 1989*, World Meteorological Organization Global Ozone Research and Monitoring Project. Rep. No. 20, Vol. II, Appendix: AFEAS Report, Geneva, Switzerland, 1990.
5. Gann, R. G., Ed., *Fire Suppression System Performance of Alternative Agents in Aircraft Engine and Dry Bay Laboratory Simulations*, NIST SP 890, National Institute of Standards and Technology, Gaithersburg, MD, 1995.
6. Miziolek, A. W., and Tsang, W., Eds., *Halon Replacements: Technology and Science*. ACS Symposium Series 611, Washington, DC, 1995.
7. Linteris, G. T., and Truett, L. F., *Combust. Flame* 105:15 (1996).
8. Burgoyne, J. H., and Williams-Lier, G., *Proc. Royal Soc.* A193:525 (1948).
9. Coleman, E. H., *Fuel* 30:114 (1951).
10. Belles, F. E., and O'Neal, C. Jr., *Sixth Symposium (International) on Combustion*, The Combustion Institute, Pittsburgh, 1957, p. 806.
11. Simmons, R. F., and Wolfhard, H. G., *Trans. Faraday Soc.* 52:53 (1956).
12. Garner, F. H., Long, R., Graham, A. J., and Badakhshan, A., *Sixth Symposium (International) on Combustion*, The Combustion Institute, Pittsburgh, 1957, p. 802.
13. Lask, G., and Wagner, H. G., *Eighth Symposium (International) on Combustion*, Williams and Wilkins, Baltimore, 1962, p. 432.
14. Rosser, W. A., Wise, H., and Miller, J., *Seventh Symposium (International) on Combustion*, Butterworths, London, 1959, p. 175.
15. Hastie, J. W., *High Temperature Vapors*, Academic Press, New York, 1975, p. 343.
16. Burgess, D. R. F., Jr., Zachariah, M. R., Tsang, W., and Westmoreland, P. R. (1995). *Thermochemical and Chemical Kinetic Data for Fluorinated Hydrocarbons*. National Institute of Standards and Technology, Gaithersburg, MD, NIST TN 1412.
17. Burgess, D. R. F., Jr., Zachariah, M. R., Tsang, W., and Westmoreland, P. R., *Thermochemical and Chemical Kinetic Data for Fluorinated Hydrocarbons, Prog. Energy Combust. Sci.* 21:453 (1996).
18. NIST WWW CKMech (Thermochemistry, Kinetics, Mechanisms) *http://fluid.nist.gov/ckmech.html*.
19. da Cruz, F. N., Vandooren, J., and Van Tiggelen, P., *Bull. Soc. Chim. Belg.* 97(11–12):1001 (1988).
20. Richter, H., Vandooren, J., and Van Tiggelen, P., *Bull. Soc. Chim. Belg.* 99(7):491 (1990).
21. Daniel, R. G., Mc Nesby, K. L., and Miziolek, A. W., *Eastern States Section Meeting, Clearwater Beach, FL, Dec. 5–7, 1994*, The Combustion Institute, Pittsburgh, 1994, p. 164.
22. Bozzelli, J. W., Tsan, H. L., Anderson, W. R., and Sausa, R. C., *Eastern States Section Meeting, Clearwater Beach, FL, Dec. 5–7, 1994*, The Combustion Institute, Pittsburgh, 1994, p. 389.
23. Westmoreland, P. R., Burgess, D. F. R. Jr., Tsang, W., and Zachariah, M. R., *Twenty-Fifth Symposium (International) on Combustion*, The Combustion Institute, Pittsburgh, 1994, p. 1505.
24. Linteris, G. T., in *Halon Replacements: Technology and Science* (A. W. Miziolek and W. Tsang, Eds.), American Chemical Society Symposium Series, Washington, DC, 1995, p. 260.
25. Battin-Leclerc, F., Walravens, B., Côme, G. M., Baronnet, F., Sanogo, O., and Vovelle, C., in *Halon Replacements: Technology and Science* (A. W. Miziolek and W. Tsang, Eds.), American Chemical Society Symposium Series, Washington, DC, 1995, p. 289.
26. Sanogo, O., Delfau, J., Akrich, R., and Vovelle, C., *Twenty-Fifth Symposium (International) on Combustion*. The Combustion Institute, Pittsburgh, 1994, p. 1489.
27. Westbrook, C. K., *Combust. Sci. Technol.* 23:191 (1980).
28. Westbrook, C. K., *Nineteenth Symposium (International) on Combustion*, The Combustion Institute, Pittsburgh, 1982, p. 127.

29. Westbrook, C. K., *Combust. Sci. Technol.* 34:201 (1983).
30. Mache, H., and Hebra, A., *Sitzungsber. Österreich. Akad. Wiss., Abt. IIa* 150:157 (1941).
31. Van Wonterghem, J., and Van Tiggelen, A., *Bull. Soc. Chim. Belg.* 63:235 (1954).
32. Andrews, G. E., and Bradley, D., *Combust. Flame* 18:133 (1972).
33. Vagelopoulos, C. M., Egolfopoulos, F. N., and Law, C. K., *Twenty-Fifth Symposium (International) on Combustion*. The Combustion Institute, Pittsburgh, 1994, p. 1341.
34. Kee, R. J., Grcar, J. F., Smooke, M. D., and Miller, J. A. (1991). *A Fortran Computer Program for Modeling Steady Laminar One-dimensional Premixed Flames*. Rep. SAND85-8240, Sandia National Laboratories, Livermore, CA.
35. Kee, R. J., Miller, J. A., and Jefferson, T. H. (1980). *CHEMKIN: A General-Purpose, Transportable, Fortran Chemical Kinetics Code Package*. Rep. SAND80-8003, Sandia National Laboratories, Livermore, CA.
36. Kee, R. J., Warnatz, J., and Miller, J. A. (1983). *A Fortran Computer Code Package for the Evaluation of Gas-Phase Viscosities, Conductivities, and Diffusion Coefficients*. Rep. SAND83-8209, Sandia National Laboratories, Livermore, CA.
37. NIST XSenkplot; An Interactive, Graphics Postprocessor for Numerical Simulations of Chemical Kinetics *http://www.nist.gov/cstl/div836/xsenkplot.*
38. Burgess, D., Jr., Tsang, W., Westmoreland, P. R., and Zachariah, M. R., *Third International Conference on Chemical Kinetics*, July 12–16, 1992, Gaithersburg, MD, 1993, p. 119.
39. Nyden, M. R., Linteris, G. T., Burgess, D. R. F., Jr., Westmoreland, P. R., Tsang, W., and Zachariah, M. R., in *Evaluation of Alternative In-Flight and Dry Bays* (W. L. Grosshandler, R. G. Gann, and W. M. Pitts, Eds.), National Institute of Standards and Technology, Gaithersburg MD, 1994, NIST SP 861, p. 467.
40. Frenklach, M., Wang, H., Yu, C.-L., Goldenberg, M., Bowman, C. T., Hanson, R. K., Davidson, D. F., Chang, E. J., Smith, G. P., Golden, D. M., Gardiner, W. C., and Lissianski, V. http://www.gri.org; and Frenklach, M., Wang, H., Goldenberg, M., Smith, G. P., Golden, D. M., Bowman, C. T., Hanson, R. K., Gardiner, W. C., and Lissianski, V. (1995). *GRI-Mech—An Optimized Detailed Chemical Reaction Mechanism for Methane Combustion*. Gas Research Institute Topical Report. No. GRI-95/0058. Chicago.
41. Zachariah, M. R., Westmoreland, P. R., Burgess, D. R. Jr., Tsang, W., and Melius, C. F., *J. Phys. Chem.*, 100:8737 (1996).
42. Zachariah, M. R., Tsang, W., Westmoreland, P. R., and Burgess, Jr., D. R. F., *J. Phys. Chem.*, 99:12512 (1995).
43. Burgess, D. R. F. Jr., and Tsang, W., personal communication, Sept. 1995.
44. Reinelt, D., and Linteris, G. T., *Twenty-Sixth Symposium (International) on Combustion*, The Combustion Institute, Pittsburgh, 1996, p. 1421.
45. Miller, D. R., Evers, R. L., and Skinner, G. B., *Combust. Flame* 7:137 (1963).
46. Benson, S. W. *J. Chem. Phys.* 38:2285 (1963).
47. Ewing, C. T., Beyler, C. L., and Carhart, H. W., *J. Fire Protection Eng.* 6(1):23 (1994).
48. Sheinson, R. S., Penner-Hahn, J. E., and Indritz, D. *Fire Safety J.* 15:437 (1989).
49. Noto, T., Babushok, V., Burgess, D. R., Hamins, A., Tsang, W., and Miziolek, A., *Twenty-Sixth Symposium (International) on Combustion*, The Combustion Institute, Pittsburgh, 1996, p. 1377.
50. Linteris, G. T., and Gmurczyk, G., in *Fire Suppression System Performance of Alternative Agents in Aircraft Engine and Dry Bay Laboratory Simulations*, (R. G. Gann, Ed.), National Institute of Standards and Technology, Gaithersburg MD, 1995, NIST SP 890, p. 201.
51. Day, M. J., Stamp, D. V., Thompson, K., and Dixon-Lewis, G., *Thirteenth Symposium (International) on Combustion*, The Combustion Institute, Pittsburgh, 1971, p. 705.
52. Dixon-Lewis, G., and Simpson, R. J., *Sixteenth Symposium (International) on Combustion*, The Combustion Institute, Pittsburgh, 1977, p. 1111.
53. Biordi, J. C., Lazzara, C. P., and Papp, J. F., *Fifteenth Symposium (International) on Combustion*, The Combustion Institute, Pittsburgh, 1975, p. 917.
54. Vandooren, J., da Cruz, F. N., and Van Tiggelen, P. J., *Twenty-Second Symposium (International) on Combustion*, The Combustion Institute, Pittsburgh, 1988, p. 1587.
55. Linteris, G. T. Unpublished results, this laboratory, 1995.
56. Smyth, K. C. Personal communication, 1995.
57. Lindstedt, P. R., in *Soot Formation in Combustion Mechanisms and Models* (H. Bockhorn, Ed.), Springer-Verlag, Berlin, 1994, p. 417.
58. Leung, K. M., and Lindstedt, P. R., *Combust. Flame* 102:129–160 (1995).
59. Seshadri, K., Mauß, F., Peters, N., and Warnatz, J., *Twenty-Third Symposium (International) on Combustion*, The Combustion Institute, Pittsburgh, 1990, p. 559.

Received 15 June 1996, accepted 20 June 1997